Symmetry breaking and electrical conductivity of $La_{0.7}Sr_{0.3}Cr_{0.4}Mn_{0.6}O_{3-\delta}$ perovskite as SOFC anode material

A. Reyes-Rojas, J. Alvarado-Flores, H. Esparza-Ponce, M. Esneider-Alcala, I. Espitia-Cabrera, E. Torres-Moye.

Abstract

This work is focused on nanocrystalline solid oxide fuel cell synthesis and characterization (SOFC) anodes of $La_{0.7}Sr_{0.3}Cr_{0.4}Mn_{0.6}O_{3-\delta}$ (perovskite-type) with Nickel. Perovskite-type oxide chemical reactivity, nucleation kinetics and phase composition related with $La_{0.7}Sr_{0.3}Cr_{0.4}Mn_{0.6}O_{3-\delta}$ –NiO to $La_{0.7}Sr_{0.3}Cr_{0.4}Mn_{0.6}O_{3-\delta}$ –Ni transformation have been analyzed. SOFC anode powders were obtained by sol–gel synthesis, using polyvinyl alcohol as an organic precursor to get a porous cermet electrode after sintering at 1365 °C and oxide reduction by hydrogen at 800 °C/1050 °C for 8 h in a horizontal tubular reactor furnace under 10% H_2/N_2 atmosphere. Composite powders were compressed into 10-mm diameter discs with 25–75 wt% Ni.

Electrical and structural characterization by four-point probe method for conductivity, scanning electron microscopy (SEM), X-ray energy dispersive spectroscopy (EDS), X-ray diffraction (XRD), and Rietveld method were carried out.

Symmetry-breaking by phase transition from high temperature aristotype R3c to hettotype I4/mmm has been identified and confirmed by XRD and Rietveld method which can be produced by introducing Ni^{2+} cations in the perovskite solid solution. Rietveld analysis suggests that Ni contents are directly proportional to

$La_{0.7}Sr_{0.3}Cr_{0.4}Mn_{0.6}NiO_{3.95}$ tetragonal structure cell volume and inversely proportional to Ni cubic structure cell volume after reduction at 1050 °C.

Kinetic analysis indicated that the Johnson–Mehl–Avrami equation is able to provide a good fit to phase transformation kinetics. The variation of electrical conductivity reveals the presence of two types of behavior in samples reduced at 1050 °C. First, at low Ni concentration (25%), ρ resistivity decreases when increasing the temperature; then, for Ni concentration higher than 25% ρ resistivity increases.

Keywords: composite materials, Sol-gel growth, Electrical conductivity, Crystal symmetry.

Introduction

Alternative energy sources have been considered as an option to reduce energy cost, because they are environment friendly and do not generate any harmful pollution. In large-scale electricity generation systems, solid oxide fuel cells (SOFC) give several advances over other fuel cell technologies since they have very high conversion efficiency (35–55%) and can be used with a wide variety of fuels [1]. Nowadays, studies have been oriented to lower operation temperature (below 800 °C) and intermediate temperature IT-SOFC (400–700 °C) [2,3].

Furthermore, significant attention has been focused on methane electro-oxidation by using anodes with different electrocatalysts including Cu, Ni, Co–CeO_2, Ni/$Ce_{1-x}Gd_xO_{2-S}$, Ni–Co/YSZ, Ni–Cu/YSZ, Cu/YSZ [4–6] and Ni–perovskite materials [7]. Perovskite $La_{0.75}Sr_{0.25}Cr_{0.5}Mn_{0.5}O_{3-s}$ is considered to be one of the most promising anodes for SOFCs operated below to 700 °C [8,9]. Additionally perovskite materials have shown promising performance for any combustible fuel including natural gas,

liquid hydrocarbons, and even solids derived from coal or biomass [10]. Ni-doped perovskite catalysts have been studied for hydrocarbon oxidation; attention has been especially focused on $La_{0.8}Sr_{0.2}Cr_{0.8}Mn_{0.2}O_{3-s}$ (LSCM), which shows suitable chemical stability but poor electrochemical performance at intermediate temperatures [11]. The majority of these investigations have been concentrated on the application of transition metals (Cu, Co, and Ni) due to their excellent electrochemical performance [12]. In addition, substitutions of lanthanum for strontium cations result in an increase of perovskite structure propane electro-oxidation [13]; but these Sr additions decrease ionic conduction [14]. In order to increase electro-oxidation performance, a slight increase of the Sr-doped was employed in this work in a perovskite $La_{0.7}Sr_{0.3}Cr_{0.4}Mn_{0.6}O_{3-s}$.

Table 1
Expected and calculated Ni concentration and cell volume, and cermet domain size. The calculated data was carried out with the Rietveld method as described in the text.

			Sample					
			LSCM1	LSCM2	LSCM3	LSCM4	LSCM5	LSCM6
	Ni(%)	Exp.	25	35	45	55	65	75
		Calc.	24.3(1)	35.4(1)	44.3(1)	54.3(1)	65.3(2)	75.2(1)
		Diff.	2.8	−1.1	1.6	1.3	−0.5	−0.3
Domain size								
	800 °C	Ni	780(5)	885(3)	>1000	>1000	>1000	>1000
Δt (nm)		ABO_3	28(1)	32(1)	29(1)	66(1)	76(1)	89(1)
	1050 °C	Ni	940(2)	>1000	>1000	>1000	>1000	>1000
		A_2BO_4	63(2)	61(1)	65(3)	110(4)	127(2)	143(3)
	Lattice							
Ni_c (Å)	800 °C	a	3.5479(1)	3.5406(1)	3.5395(1)	3.5357(2)	3.5311(1)	3.5310(1)
ABO_{3h} (Å)		a	5.4968(1)	5.4968(1)	5.4961(1)	5.4960(1)	5.4965(1)	5.4971(1)
		c	13.4101(1)	13.4101(1)	13.4439(1)	13.4442(1)	13.4451(1)	13.4458(1)
Ni_{c^*} (Å)	1050 °C	a	3.5479(1)	3.5408(1)	3.5396(1)	3.5359(2)	3.5310(1)	3.5311(1)
A_2BO_{4t} (Å)		a	3.8565(1)	3.8464(1)	3.8661(1)	3.8594(1)	3.8688(1)	3.8671(1)
		c	12.6291(1)	12.7007(1)	12.6122(1)	12.6594(1)	12.5990(1)	12.6452(1)
Volume cell (Å^3)	800 °C	Ni_c	44.661(1)	44.384(1)	44.343(1)	44.200(1)	44.029(1)	44.028(1)
		ABO_{3h}	350.905(1)	350.905(1)	351.694(1)	351.747(1)	351.776(1)	351.882(1)
	1050 °C	Ni_{c^*}	44.661(1)	44.394(1)	44.348(1)	44.211(1)	44.028(1)	44.029(1)
		A_2BO_4	187.833(1)	187.914(1)	188.514(1)	188.562(1)	188.584(1)	189.107(1)
	Porosity Φ (%)		42(2)	44(2)	45(2)	45(1)	46(1)	46(1)

(c) cubic phase, (h) hexagonal phase, (t) tetragonal phase; c, h at 800 °C and c^*, t at 1050 °C.
The number between parenthesis represents the error of last number.

Ni is used in SOFCs because of its excellent electro-catalytic activity for H_2 oxidation reaction and high electrical conductivity [15]. Moreover, when used with hydrocarbons at high temperature, CO electrochemical oxidation at the surface of oxide anode must be fast enough to prevent coke deposit formation (C–C bond) [16]. Reduced carbon deposition was reported at lower temperature in cermets with high Ni content by introducing a small quantity (1%) of molybdenum [17]. It is known that perovskite oxides $LaMO_3$ (M= Cr, Mn) show high catalytic activities for CO oxidation [18]. Therefore, as an alternative $La_{0.7}Sr_{0.3}Cr_{0.4}Mn_{0.6}O_{3-S}$ perovskite can be used with additions of Ni and study the dynamics of these transformations by Rietveld method and their relation with electrical properties for the possible application of these devices.

Recent studies have reported high electrochemical activity in $La_{0.6}Sr_{0.4}Fe_{0.8}Co_{0.2}O_{3-S}$ perovskite dispersed on NiO particles [19]. However their crystal structure was partially modified in La_2NiO_4 and $Sr(Fe_{0.5}Co_{0.5})O_{2.88.}$ In these transition-metal oxides, NiO reduction of by H_2 has been the object of the most extensive studies [20], because NiO appears as a component in many oxidation catalysts [21]; but when oxide is surrounded by other crystal structures the mechanism for oxide reduction can be modified.

In order to elucidate the relationship between Ni and crystal structure variation a composite anode $La_{0.7}Sr_{0.3}Cr_{0.4}Mn_{0.6}O_{3-S}$–NiO has been studied by TRXRD in situ under H_2 atmosphere.

In the perovskite–Ni composite anode, Ni acts both as a catalyst and an electronic conducting crystal structure, while perovskite structure mainly acts as a matrix and catalyst. Perovskite structure materials can also improve anode

electrochemical oxidation activity, especially when using hydrocarbon fuels. It has been demonstrated that triple-phase boundary length (TPB) correlates well with the reaction rate for hydrogen electrochemical oxidation; thus, TPB length becomes a determining factor in improving anode efficiency [22]. Therefore, this can be reached by optimizing Ni–perovskite composite anode microstructure through the adjustment of powder morphologies and particle sizes for Ni and perovskite precursors developing a favorable electrochemical process.

In this work phase transformations and dynamics that take place during $La_{0.7}Sr_{0.3}Cr_{0.4}Mn_{0.6}O_{3-S}$–NiO→$La_{0.7}Sr_{0.3}Cr_{0.4}Mn_{0.6}O_{3-S}$- Ni reduction and electrical conductivity are analyzed. A detailed structural analysis has been performed through X-ray diffraction and Rietveld method. Their structural and chemical characterization during isothermal reduction was analyzed by in situ TRXRD which allowed knowing the reduction kinetic process. Also, the influence of Ni/LSCM content on kinetics and electrical conductivity behavior was examined. Microstructure was observed by scanning electron microscopy (SEM) and its chemical composition was obtained by X-ray energy dispersive spectroscopy (EDS).

Experimental

Sample preparation by the sol-gel method: Series of the perovskite-type $La_{0.7}Sr_{0.3}Cr_{0.4}Mn_{0.6}O_{3-S}$–Ni compounds with concentrations ranging from 25 to 75 wt% Niwere prepared by sol–gel method. Stoichiometric amounts of nickel acetylacetonate $Ni(C_5H_7O_2)_2Ni{\cdot}2H_2O$ (>99.9% purity Aldrich), lanthanum acetylacetonate $La(CH_3COCHCOCH_3)_3{\cdot}xH_2O$ (>99.9% purity Aldrich), strontium acetate $(CH_3CO_2)_2Sr$ (>99.9% purity Aldrich), chromium(III) acetylacetonate $Cr(C_5H_7O_2)_3$ (>99.9% purity

Aldrich) and manganese (II) acetylacetonate [$CH_3COCH= C(O)CH_3]_2Mn$ >99.9% purity Aldrich, were used to obtain six cermets (see Table 1). Precursors were dissolved in "deionized water–nitric acid HNO_3", ethanol C_2H_5OH, deionized water, "nitric acid HNO_3–deionized water" and "butanol $H_3C(CH_2)_3OH$–acetic acid $C_6H_8O_7H_2O$" respectively to form homogenous, steady and transparent sol solutions at 60 °C. Dissolved ion solutions were mixed homogenously by stirring, reflux and heating at the same temperature. Ethylene glycol $C_2H_6O_2$ was added to each sol for the enhancement of salt dissolution. The solution pH value was tuned to 3 by adding ammonia solution. Hydrolysis and condensation reaction were accomplished by refluxing the mixed solution for 12 h. Gels were obtained by slow evaporation at 70 ◦C until dried gel was formed. The gel was dried at 120 °C during 12 h and then calcined at 800 °C for 1 h in air.

Polyvinyl alcohol was used as pore-former in all cermets, which keeps a constant pore volume throughout the sample. The samples were milled in an agate mortar during 1 hour, and the obtained powders were afterwards compressed into 1-cm-in-diameter discs with 1mm in thickness using a 1-ton unidirectional axial pressure for 5 s, and drying them at 110 °C during 24 h. Afterwards, the discs were calcinated from room temperature to 800 °C with a heating rate of 1 °C/min in an atmospheric air-heated box furnace for 2 h. Once the pore was formed, disc samples were sintered at 1365 °C for 1 h with a heating rate of 5 °C/min. The cooling rate for each anode was 5 °C/min. Once the sintered samples were obtained, each one was reduced in a horizontal furnace at 800 °C under 10% H_2 in N_2 atmosphere with a flow ≈150cm^3/min. The atmosphere was being reduced during cooling to inhibit oxidation layer formation on the cermet surface.

Characterization: Once the reduction process was concluded, each sample was analyzed by using an X-ray powder diffractometer model X'Pert MPD Phillips, with Cu Kα monochromatic radiation and θ–2θ geometry. Powder XRD patterns were obtained from 20 to 80° 2θ angle range in step-scanning mode with a step length of 0.05° and a stepcounting time of 10 s. Crystal structure and symmetry parameters were obtained by the Rietveld method with the FULLPROF program [23]. Peak shape modified Thompson–Cox–Hasting pseudo-Voigt function was used for simulation of XRD reflection profile.

In order to obtain high-precision reproducibility; background parameters, scale factors, instrumental effects, structural parameters, profile parameters, domain size parameters, and crystal structure quantification were considered for refinement until results converged into minimum values. Instrumental broadening U, V, and W was determined by Rietveld refinement of an X-ray diffraction pattern of an Al_2O_3 powder standard for quantitative analysis [24]. Values obtained from refinement were used in all patterns (U= 0.01951, V =−0.030181, and W= 0.015934). Crystal structure data for all patterns was obtained from well-known Refs. [25–27].

Kinetic data and solid state crystallization were obtained by in situ TRXRD at 800 °C and 1050 °C in a 10% H_2 and 90% N_2 atmosphere, with a flow ≈150cm^3/min. Therefore, in order to enhance phase transformation kinetics a $La_{0.7}Sr_{0.3}Cr_{0.4}Mn_{0.6}O_{2.85}$–NiO cermet with 75 wt% NiO and 25 wt% $La_{0.7}Sr_{0.3}Cr_{0.4}Mn_{0.6}O_{2.85}$, was mixed with ethyl alcohol and a drop was placed on Xray powder diffractometer heating holder (model D5000 Siemens, equipped with Cu Kα monochromatic radiation, θ–θ geometry and with a PSD detector). In situ reduction from NiO–$La_{0.7}Sr_{0.3}Cr_{0.4}Mn_{0.6}O_{2.85}$ to Ni–

$La_{0.7}Sr_{0.3}Cr_{0.4}Mn_{0.6}O_{2.85}$ and cermet time reduction were obtained by collecting an individual diffraction pattern each 20 min, in periods of 8 h each by using a PSD-50m MBRAUN. All XRD patterns were refined with the Rietveld method to quantify the amount of transformed phase y(t) and to determine reaction-rate constant.

Effective porosity (Φ) was obtained by using cystallographic density ρ_c (calculated from the volume data obtained by Rietveld analysis); according the following equation:

$$\phi = 1 - \left(\frac{\rho}{\rho_c}\right) \qquad (1)$$

Where ρ is bulk density.

$La_{0.7}Sr_{0.3}Cr_{0.4}Mn_{0.6}O_{2.85}$–Ni cermets electrical conductivity was investigated using the four-point probe Van Der Pauw method [28] from room temperature to 800 °C, in a horizontal tubular furnace equipped with Hewlett Packard 3497OA digital multimeters and with data acquisition for temperature and electrical resistivity. All cermets were measured in a continuous flow ≈150cm^3/min of 10% H_2/N_2 gas (Praxair, 99.9%).

The micro-structural evolution and chemical composition data of the cermets were obtained by using a JEOL-5600 Scanning Electron Microscope (SEM) in which an EDS EDAX equipment is attached and a transmission electron microscope (TEM) Philips CM200.

Results and discussion

Rietveld analysis and porosity: Powder XRD patterns of the samples $La_{0.7}Sr_{0.3}Cr_{0.4}Mn_{0.6}O_{2.85}$–Ni prepared from 25% Ni to 75% Ni indicated its amorphous nature at 120 °C (dried gel). Crystal structure formation of the sintering samples in air at

1365 °C for 1 h shows essentially crystallographic planes of the crystal family hexagonal perovskite $La_{0.7}Sr_{0.3}Cr_{0.4}Mn_{0.6}O_{2.85}$ and NiO cubic structure. Results with the Rietveld method for $La_{0.7}Sr_{0.3}Cr_{0.4}Mn_{0.6}O_{3-S}$–Ni compounds were obtained using the space group R3c for hexagonal phase, I4/mmm for the tetragonal phase and Fm3m for the cubic phase [29]. As an example, Fig. 1A shows the final cermet fitting with 45% Ni (sample LSCM3) after the first cycle of reduction process at 800 °C in H_2–N_2 a atmosphere; clearly confirms the formation of $La_{0.7}Sr_{0.3}Cr_{0.4}Mn_{0.6}O_{2.85}$ perovskite structure and the absence of NiO crystals. The experimental profile was indicated by (+), the cal culated one by (−), and the difference plot between the observed and calculated intensities are shown in each case. In these figures, an acceptable adjustment for the differences between the observed and calculated profile intensities was registered. Perovskite structure is not altered by this treatment. However when the cermets were treated by a second cycle of reduction at 1050 °C, perovskite crystal structure is clearly altered from $La_{0.7}Sr_{0.3}Cr_{0.4}Mn_{0.6}O_{2.85}$ to A_2BO_4 type structure [30] (see Fig. 1B). As it is observed in Fig. 1, almost flat differences were obtained between the observed and calculated profile intensities. Adjustment degree for fitting patterns was from 5 to 10 (R_{wp}).

At 800 °C the phase is hexagonal perovskite and contains six formula units per unit cell. However, at 1050 it has only two formula units per cell. This leads to an oxygen content reduction from 0.58% to 0.56%. Assuming $La_{0.7}Sr_{0.3}Cr_{0.4}Mn_{0.6}NiO_{3.95}$ and Ni as the main reduction products of the reaction, the possible reaction mechanism with S = 0.15 can be considered as follows:

$$La^{3+}_{0.7}Sr^{2+}_{0.3}Cr^{3+}_{0.4}Mn^{3+}_{0.6}O^{2-}_{2.85} + Ni^{2+}O^{2-} + H^{1+}_2 \rightarrow La^{3+}_{0.7}Sr^{2+}_{0.3}Cr^{2+}_{0.4}Mn^{4+}_{0.6}Ni^{2+}O^{2-}_{3.95} + Ni^{3+} + (1.15-\delta)H^{1+}_2O^{2-} \quad (2)$$

Recent studies have shown that perovskite structure can be stabilized by low-level doping with Ni [31]. However, this study indicated that excessive amounts of Ni contained in the solid solution causes symmetry-breaking. XRD patterns with A_2BO_4 type structure were refined on a lower symmetry body centered tetragonal crystal structure, consistent with a structure $La_{0.7}Sr_{0.3}Cr_{0.4}Mn_{0.6}NiO_{3.95}$ (I4/mmm). This lowering of symmetry by phase transition from aristotype R3c to hettotype I4/mmm can be caused by the tilting of adjacent layers of the rigid BO_6 octahedra about the threefold rotation axes of hexagonal perovskite [32,33]. Thus, the obtained results support the symmetry proposed for structures type perovskite with tilted octahedra and distortion from R3c (anti-phase) to I4/*mmm* (in-phase) [34]. The presence of O vacancies leads to an increase in adsorption energy of H_2 and substantially lowers the energy barrier associated with the H–Hbond cleavage [20]. Therefore, displacement of $<La^{3+}–Sr^{2+}>$ and $<Cr^{3+}\text{-}Mn^{3+}>$ cations by the presence of O vacancies and incorporation of Ni^{2+} cations along crystallographic directions [2 2 1] off center can induce a phase transformation mechanism to the new tetragonal phase; only in a controlled and reduced atmosphere (10% H_2/N_2). Acceptable and good adjustment for the differences between the observed and calculated profile intensities was registered. Fig. 1B shows the final cermet fitting with 45% Ni (sample LSCM3) calculated by the Rietveld method after second treatment.

The percentage of Ni in each of the 6 samples after reduction process is indicated in Table 1 together with the one calculated with Rietveld method and cermet domain size (Δt). Some differences were observed for the average domain size between samples treated at 800 °C and 1050 °C. Ni crystals domain size at 800 °C

does not change considerably (around 780 nm) for samples with 25% and 35% of Ni after the reduction process, whereas in the rest of the samples it increases to >1000 nm. nm.When temperature was increased to 1050 °C, the domain size was 940nm for the 25% Ni sample, and the rest increased to >1000nm too. This behavior is normal due to grain coalescence of elongated grains of Ni [35–37]. However, the rhombohedral perovskite phase domain size (ABO_3) increased from 28nm (25% Ni) to 89nm (75% Ni) at 800 °C, whereas for the tetragonal phase (AB_2O_4, 1050 °C) it was from 63nm (25% Ni) to 143nm (75% Ni), almost twice (see Table 1). Domain size increase can be directly related to Ni amount and its nucleation to form tetragonal structure.

Crystal structure data for Ni obtained with Rietveld analysis during the reduction process at 800 °C showed a slight change in lattice parameters and cell volume. Table 1 shows a decrement in Ni cubic unit cell volume when Ni% increased after the reduction process. Ni structure cell volume decreased from 44.661 $Å^3$ to 44.028 $Å^3$. It can be explained by oxidation states; taking into account the Ni different ionic radius, which can be changed from Ni^{2+}(0.69 Å) to Ni^{+3} (0.55Å), volume decrease results in the increasing content of the smaller Ni^{3+} cations which dimensions of the lattice might be compensated by larger Ni^{2+} cations. During the second reduction process at 1050 °C, cermets Ni cell volume was quite comparable.

Crystal structure data for $La_{0.7}Sr_{0.3}Cr_{0.4}Mn_{0.6}O_{2.85}$ obtained with Rietveld analysis during the reduction process at 800 °C shows a change in lattice parameters and a slight increase in cell volume. This small increase of unit cell volume may be a consequence of entering larger Ni^{2+} cations in perovskite structure [31,38].

However, during the reduction process at 1050 °C the $La_{0.7}Sr_{0.3}Cr_{0.4}Mn_{0.6}NiO_{3.95}$ crystal structure showed a unit cell parameter distortion (a, b) and a slight increase in cell volume too. This behavior can be explained through cations interchange, which is ordered in amore close-packed A_2BO_4 tetragonal structure when Ni content increases in $La_{0.7}Sr_{0.3}Cr_{0.4}Mn_{0.6}NiO_{3.95}$–Ni compounds.

The Rietveld analysis suggests that Ni contents are directly proportional to $La_{0.7}Sr_{0.3}Cr_{0.4}Mn_{0.6}NiO_{3.95}$ tetragonal structure cell volume and inversely proportional to Ni crystal structure cell volume after reduction at 1050 °C with H_2–N_2 atmosphere for 8 h.

Furthermore, anode porosity was proportional to the cermet NiO amount. This increase can be attributed to Ni amount and volume size change during the reduction process. 25 wt% Ni (LSCM1) cermet porosity was around 40%. Its adequate to optimize triple phase boundary and increase electro-oxidation reaction of the SOFC's anodes [39].

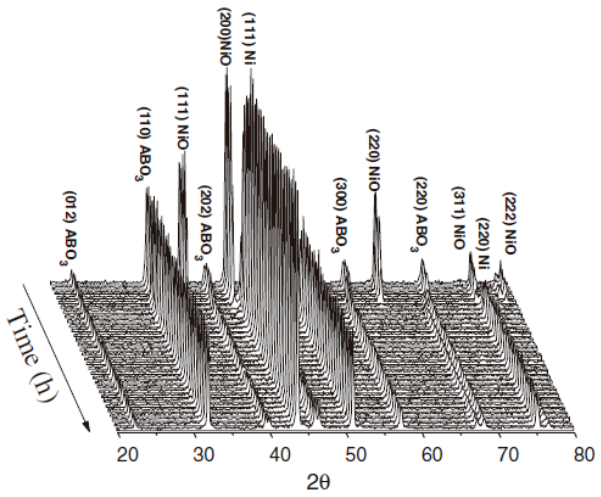

Fig. 2. Time-resolved XRD for the isothermal reduction $La_{0.7}Sr_{0.3}Cr_{0.4}Mn_{0.6}O_{2.85}$–NiO → $La_{0.7}Sr_{0.3}Cr_{0.4}Mn_{0.6}O_{2.85}$–Ni at 800 °C under N–$H_2$ atmosphere (sample LSCM6).

Fig. 2 shows an hkl relative intensity plot vs. diffraction angle for $La_{0.7}Sr_{0.3}Cr_{0.4}Mn_{0.6}O_{2.85}$–NiO→$La_{0.7}Sr_{0.3}Cr_{0.4}Mn_{0.6}O_{2.85}$–Ni at 800 °C ($ABO_3$ +AO→A_2BO_4, LSCM6) isothermal reduction reaction. (1 1 1)NiO X-ray crystallographic reflection intensity decreases while a symmetrical and simultaneous (1 1 1)Ni plane increases during the first 60 min, but only after an induction period of 10 min. After 120 min, $(1\ 1\ 1)_{NiO}$ plane intensity continuously decreases but at a slow rate and $(1\ 1\ 1)_{Ni}$ plane intensity increases at the same rate. During the first 180 min the reaction was completed. Crystal structure for both phases remains unchanged for 8 h after reduction process.

Similar behavior was obtained by thermogravimetric techniques for other authors in compounds with NiO reduced to temperatures lower than 1000 °C [40], however, the maximum reduction rate is smaller than $La_{0.7}Sr_{0.3}Cr_{0.4}Mn_{0.6}O_{2.85}$–Ni. Therefore, high and lower profile reduction can be obtained by $La_{0.7}Sr_{0.3}Cr_{0.4}Mn_{0.6}O_{2.85}$ content, because they are surrounding the NiO particles. This behavior is not obtained in works with single NiO particles underH_2 reduction; therefore there is a diffusion problem [41].

Kinetic analysis and microstructure: In order to elucidate the transformation phase at 800 °C and 1050 °C and to get the proper reaction mechanism, reaction order and reaction rate kinetic parameters were obtained by using the Johnson–Mehl–Avrami (JMA) theory [42], where the reacted fraction y(t) is given as a function of time t, by

$$y(t) = 1 - \exp[-(kt)^n], \qquad (3)$$

where k is the temperature-dependent rate parameter and n is the reaction order.

Kinetic parameters such as concentration y(t) were calculated by Rietveld method and the reaction rate can be determined through the relations [43]:

$$y_\alpha(t) = 1 - \frac{C_\alpha(t)}{C_\alpha(0)} \quad (4)$$

$$y_\beta(t) = \frac{C_\beta(t)}{C_\beta(\infty)} \quad (5)$$

where α and β are the fraction consumed and formed at any time t respectively.

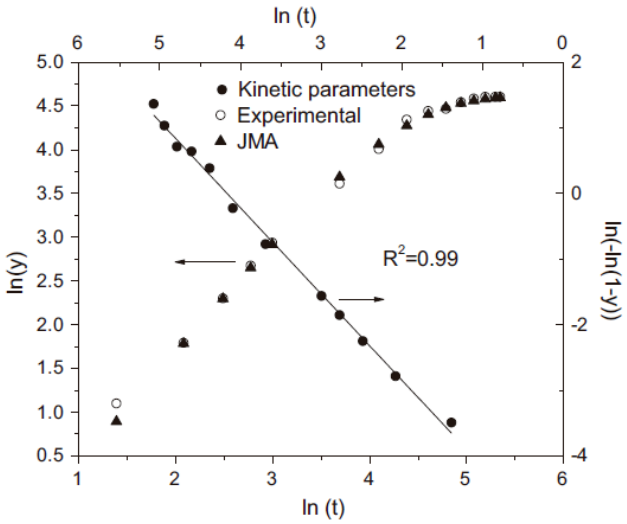

Fig. 3. Reaction kinetics from the TRXRD analysis fitted by Johnson–Mehl–Avrami equation in $La_{0.7}Sr_{0.3}Cr_{0.4}Mn_{0.6}O_{2.85}$–Ni system.

The experimental and isothermal fractional data y(t) obtained from TRXRD is shown in Fig. 3. It is seen that the rate of conversion increases at the beginning and decreases after the flex point and tends to zero when the transformation goes to completion; after subtraction of the induction period the growth is a diffusioncontrolled process.

Data point dependence of ln[ln(1−y)] on ln(t) gives a straight line (R^2 = 0.99) in the whole investigated dwell time region, meaning that NiO particles decomposition in $La_{0.7}Sr_{0.3}Cr_{0.4}Mn_{0.6}O_{2.85}$ perovskite composite obeyed to the JMA equation well. The

linear fit of experimental data gives an Avrami exponent n close to 1 (1.3) and a constant rate of k = 0.004 min^{-1} during the $La_{0.7}Sr_{0.3}Cr_{0.4}Mn_{0.6}O_{2.85}NiO \rightarrow La_{0.7}Sr_{0.3}Cr_{0.4}Mn_{0.6}O_{2.85}$–Ni reduction reaction at 800 ◦C.

Fig. 4 displays time resolved XRD data under isothermal conditions at 1050 °C for 8 h after reduction process at 800 °C. During the first 2 h, no major changes are seen in reflection profile intensity for $La_{0.7}Sr_{0.3}Cr_{0.4}Mn_{0.6}O_{2.85}$, therefore, perovskite crystal structure remains unchanged. However, after this incubation period exhibits symmetry breaking; perovskite crystallographic planes then begin to disappear and simultaneously crystallographic planes for tetragonal $La_{0.7}Sr_{0.3}Cr_{0.4}Mn_{0.6}NiO_{3.95}$ appear without diffraction features for an intermediate suboxide crystal structure. It showed that the time taken to complete symmetry breaking reaction was 2 h after incubation period. After this time tetragonal structure remains unchanged. This crystal structure transformation by splitting of the hexagonal (1 1 0) reflection into (1 1 0)/(1 0 3) tetragonal structure doublet can be due to the relative stability of the Mn^{3+} on the surface (first layer) and subsurface (second layer) regions of (0 0 l) hexagonal structure which induce the beginning of cation movement (La^{3+}, Sr^{2+}, Cr^{3+}) to O vacancies stability and to perovskite interaction with Ni at high temperature withH_2 atmosphere, which is re-ordered in a new structure with an oxygen reduction of 2% in a closer-packed A_2BO_4 tetragonal structure.

All the cermets' microstructure observed with TEM and SEM before and after the reduction process was very similar. In Fig. 5 anode microstructure with 25 wt% Ni before and after reduction process is shown. Morphological analysis showed that the cermets had the same morphology and an average perovskite particle size of

approximately 0.5μm. Perovskite structure particles analyzed with EDS, were observed surrounding NiO particles. These NiO particles have sizes from 1 to 2μm. These observations are consistent with the reduction process kinetics behavior, which is obstructed by perovskite particles.

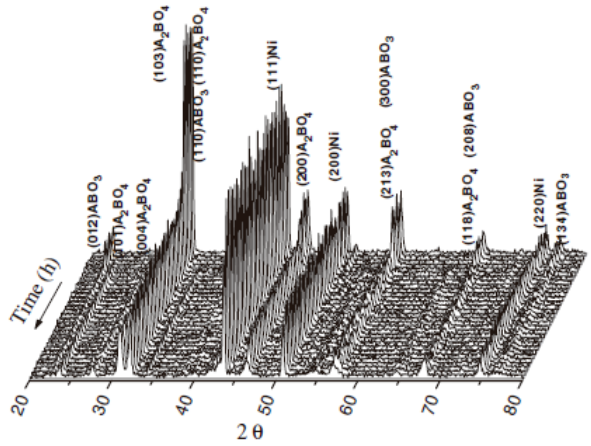

Fig. 4. Time-resolved XRD for the isothermal reduction $La_{0.7}Sr_{0.3}Cr_{0.4}Mn_{0.6}O_{2.85}$–Ni → $La_{0.7}Sr_{0.3}Cr_{0.4}Mn_{0.6}NiO_{3.95}$–Ni at 1050 °C under N–$H_2$ atmosphere (sample LSCM6).

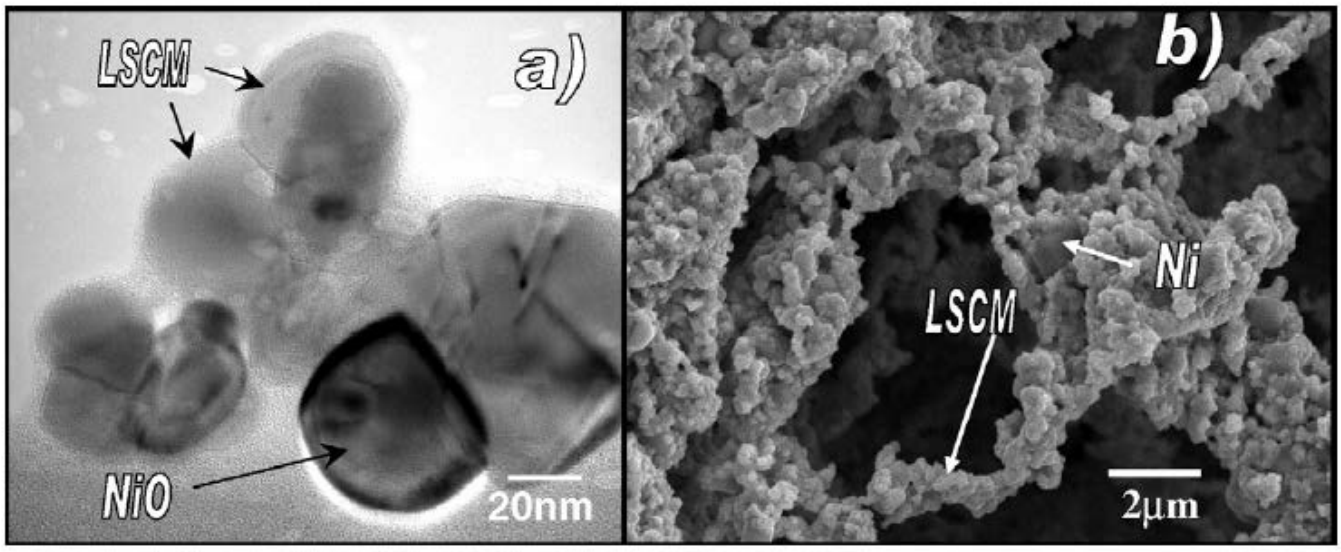

Fig. 5. TEM and SEM images of sample LSCM1 cermets composite sintered at 1365 °C for 1 h in air. Before (a) and after (b) reduction process.

Electrical conductivity: Electrical conductivity of cermets isothermally crystallized at 800 °C and 1050 °C was measured in function of Ni content according to $La_{0.7}Sr_{0.3}Cr_{0.4}Mn_{0.6}O_{2.85}$ content in H_2, and a direct effect of the $La_{0.7}Sr_{0.3}Cr_{0.4}Mn_{0.6}NiO_{3.95}$ phase formation on cermets' electrical properties was found.

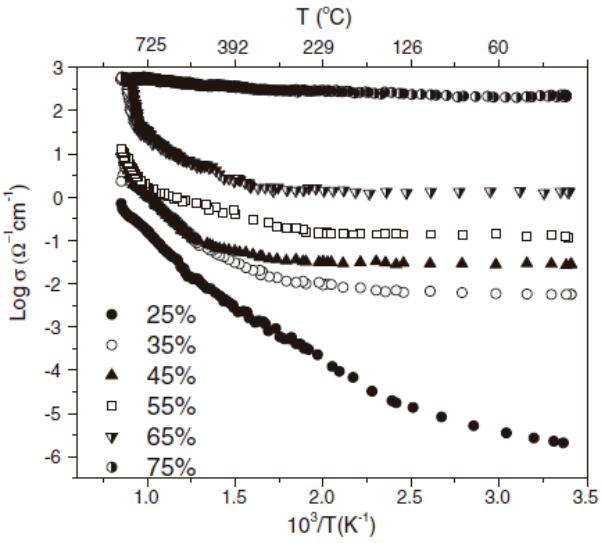

Fig. 6. Log σ vs $1/T$ graphs for $La_{0.7}Sr_{0.3}Cr_{0.4}Mn_{0.6}O_{2.85}$–Ni cermets at 800 °C with H_2–N_2 atmosphere.

Cermet electrical conductivity behavior obtained by 4-probe measurements from room temperature to 800 °C is plotted in Fig. 6. This figure represents a semiconductortype behavior for the samples from 25 to 75 wt% of Ni. The change of electrical conductivity in Fig. 6 can be attributed to the height increment of Ni, because when nickel increases electrical conductivity too; electrical conductivity is significantly lowered in low Ni concentrations ($<<1\Omega^{-1}cm^{-1}$). Ni compositions from 65 to 75% show a tendency to form a maximum in conductivity dependence versus temperature ($\sim 3\Omega^{-1}$ cm^{-1}). On the contrary, Ni compositions from 25 to 55% show a tendency to conductivity minimums in the whole temperature range 25–800 °C. For $La_{0.7}Sr_{0.3}Cr_{0.4}Mn_{0.6}O_{2.85}$–Ni based phases, the experimental conductivity tendency data suggest that samples with

35 and 45% of Ni are more closed for SOFC anode applications [12,44]. Also, other studies indicated that Ni in anode electrode increases the polarization resistance when concentration exceeded the 50% [45].

On the contrary, isothermally crystallized cermets at 1050 °C showed a semiconductor-type behavior when the Ni concentration was 25%. However, when Ni concentration increases, the electrical conductivity profile changes from semiconductor to metallic-type behavior (see Fig. 7). This study indicates that metallic-type behavior ior dominates when Ni concentration increases from 35 to 75%. Thus, our results support the conductivity behavior proposed for tetragonal structures type $La_2Cu_{0.7}Co_{0.3}O_{4+S}$ [46,47] whereas Ni concentration does no go over 25%. After this value the process is controlled by ametallic-type behavior. Unambiguously the brokensymmetry from hexagonal perovskite ($La_{0.7}Sr_{0.3}Cr_{0.4}Mn_{0.6}O_{2.85}$) to tetragonal structure ($La_{0.7}Sr_{0.3}Cr_{0.4}Mn_{0.6}NiO_{3.95}$) showed a drastic diminution of electrical conductivity.

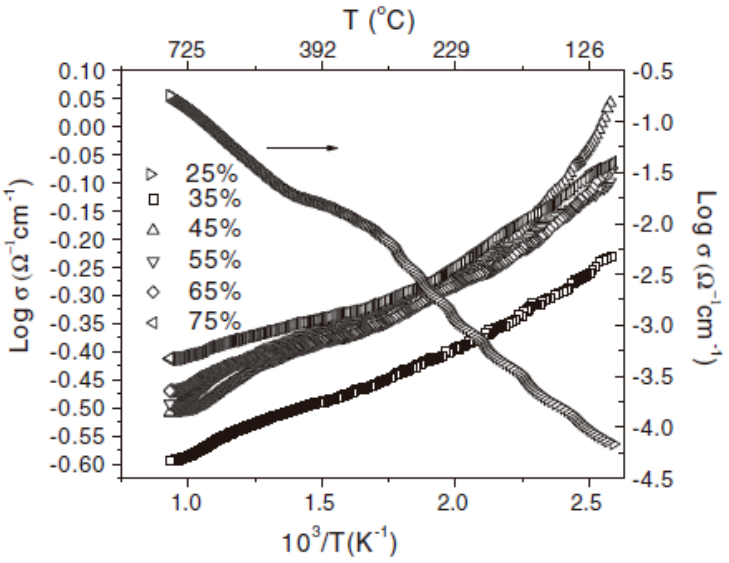

Fig. 7. Log σ vs $1/T$ graphs for $La_{0.7}Sr_{0.3}Cr_{0.4}Mn_{0.6}NiO_{3.95}$–Ni cermets at 1050 °C with H_2–N_2 atmosphere.

Conclusions

Composites of $La_{0.7}Sr_{0.3}Cr_{0.4}Mn_{0.6}O_{2.85}$–Ni cermets with good electrical properties were synthesized by sol–gel method and the chemical reactivity of perovskite oxide SOFC anodes under a H_2 atmosphere was evaluated its possible application as anode in solid oxide fuel cells. The results of in situ timeresolved XRD show a direct $La_{0.7}Sr_{0.3}Cr_{0.4}Mn_{0.6}O_{2.85}$–NiO→$La_{0.7}Sr_{0.3}Cr_{0.4}Mn_{0.6}O_{2.85}$–Ni transformation without accumulation of any intermediate crystal structure at 800 °C. Reduction Kinetics in these cermets follows a high and low profile reduction while hexagonal perovskite particles are surrounding and then reduction process is obstructed, therefore there is a diffusion problem. When increasing the temperature to above 1050 °C, the symmetrybreaking defect can be produced by introducing Ni^{2+} cations in the perovskite solid solution, but only after an induction period. Surface sites defects may be created by adsorption ofH_2 and by oxygen vacancies which induce cation movement and a phase transformation mechanism to the new tetragonal phase.

The results of electrical conductivity and phase transformation kinetics in Ni–$La_{0.7}Sr_{0.3}Cr_{0.4}Mn_{0.6}O_{2.85}$–Ni anodes, compared with other works, allow us to conclude that samples with 35 wt% and 45 wt% of Ni phase are the most acceptable material for application as anode in solid oxide fuel cells due to their similar performance.

Acknowledgments

The authors would like to thank Raul A. Ochoa and D. Lardizábal for their valuable participation in this work. We also want to thank Centro de Investigación en Materiales Avanzados S.C. for the facilities for this work. This work was supported by project CONACYT No. 105837.

References

[1] Daniele Cocco, Tola Vittorio, Energy Convers. Manage. 50 (2009) 1040.

[2] Ashok Kumar Baral, V. Sankaranarayanan, Appl. Phys. A – Mater. Sci. Process 98 (2010) 367.

[3] Feng-Yun Wang, Guo-Bin Jung, Sub Ay, Shih-Hung Chan, Xiao Hao, Yu-Chun Chiang, J. Power Sources 185 (2008) 862.

[4] Li Yongxin, Guo Yuhua, Xue Bing, Fuel Process. Technol. 90 (2009) 652.

[5] Shaowu Zha, William Rauch, Meilin Liu, Solid State Ionics 166 (2004) 241.

[6] A. Ringuede, J.A. Labrincha, J.R. Frade, Solid State Ionics 141–142 (2001) 549.

[7] Lo Faro Massimiliano, La Rosa Daniela, Isabella Nicotera, Antonucci Vincenzo, Salvatore Arico Antonino, Appl. Catal. B – Environ. 89 (2009) 49.

[8] Shanwen Tao, T.S. Irvine John, Nat. Mater. 2 (2003) 320.

[9] J. Pe˜na-Martinez, D. Marrero-Lépez, D. Pérez-Coll, J.C. Ruiz-Morales, P. Ni˜nez, Electrochim. Acta 52 (2007) 2950.

[10] A.C. Mai Andreas, Haanappel Vincent, Uhlenbruck Sven, Tietz Frank, Stover Detlev, Solid State Ionics 176 (2005) 134.

[11] Jiang Liu, Brian D. Madsen, Ji Zhiqiang, Scott A. Barnett, Electrochem. Solid State Lett. 5 (6) (2002) A122.

[12] J. Wan, J.H. Zhu, J.B. Goodenough, Solid Sate Ion. 177 (2006) 1211.

[13] T. Hirano, H. Purwanto, T. Watanabe, T. Akiyama, J. Alloys Compd. 441 (2007) 263.

[14] V.V. Kharton, A.L. Shaulo, A.P. Viskup, M. Avdeev, A.A. Yaremchenko, M.V. Patrakeev,

A.I. Kurbakov, E.N. Naumovich, F.M.B. Marques, Solid State Ionics 150 (2002) 229.

[15] S. Primdahl, M. Mogensen, Solid State Ionics 152–153 (2002) 597.

[16] J. McIntosh Stevenn, Gorte Raymond, Chem. Rev. 104 (10) (2004) 4845.

[17] Joon-Ho Koh, Young-Sung Yoo, Jin-Woo Park, Chun Hee Lim, Solid State Ionics 149 (2002) 157.

[18] W.F. Libby, Science 171 (1971) 499.

[19] Maximiliano Lo Faro, Daniela La Rosa, Isabella Nicotera, Vincenzo Antonucci, Antonio Salvatore Arico, Appl. Catal. B – Environ. 89 (2009) 49.

[20] Tae-Yeol Jeon, Sung Jong Yoo, Yong-Hun Cho, Soon Hyung Kang, Yung-Eun Sung, Electrochem. Commun. 12 (2010) 1796.

[21] B. Jankovic, B. Adnadevic, S. Mentus, Chem. Eng. Sci. 63 (2008) 567.

[22] K.K. Hansen, K. Hansen Vels, Solid State Ionics 178 (2007) 1379.

[23] J. Rodriguez-Carvajal, 2007 Wfp2k Rietveld Program, version 2007, Laboratorie Leon Brillouin (CEA-CNRS).

[24] National Institute of Standards and Technology 1989 Standard Reference Material 674a, Department of Commerce, United States of America.

[25] JCPDS-International Centre for Diffraction Data, Copyright (C) JCPDS-ICDD 2008, card 01-089-7128.

[26] JCPDS-International Centre for Diffraction Data, Copyright (C) JCPDS-ICDD 2008, card 01-089-4461.

[27] JCPDS-International Centre for Diffraction Data, Copyright (C) JCPDS-ICDD 2008, card 01-081-2084.

[28] L.J. Van der Pauw, Philips Res. Rep. 13 (1958) 1.

[29] International Tables for Crystallography, 1996.

[30] Inorganic Crystal Structure Database ICSD version 2009-1 (atomic positions).

[31] V.V. Vashook, D. Franke, J. Zosel, K. Ahlborn, L. Vasylechko, W. Fichtner, U. Guth, Solid State Ionics 179 (2008) 135.

[32] A.M. Glazer, Acta Cryst. B28 (11) (1972) 3384.

[33] M.T. Dove, Am. Mineral. 82 (1997) 213.

[34] C.N.W. Darlington, Acta Cryst. A58 (2002) 299.

[35] S. Deki, H. Yanagimoto, S. Hiraoka, K. Akamatsu, K. Gotoh, Chem. Mater. 15 (26) (2003) 4916.

[36] D. Farkas, A. Frøseth, H. Van, Scripta Mater. 55 (2006) 695.

[37] M.H. Pihlatie, H.L. Frandsen, A. Kaiser, M. Mogensen, J. Power Sources 195 (2010) 2677.

[38] A.L. Sauvet, J.T.S. Irvine, Solid State Ionics 167 (2004) 1.

[39] J.H. Lee, H. Moon, H.W. Lee, J. Kim, D.D. Kim, K.H. Yoon, Solid Sate Ion. 148 (2002) 15.

[40] M. Bahgat, Min-Kyu Paek, Jong-Jin Pak, J. Alloys Compd. 472 (2009) 314.

[41] Haifeng Wang, Feng Liu, Tao Zhang, Gencang Yang, Yaohe Zhou, Acta Mater. 57 (2009) 3072.

[42] M. Avrami, J. Chem. Phys. 7 (1939) 1103.

[43] D.D.L. Chung, W. Patrick, H. DeHaven, Arnold, Debastis Ghosh, X-ray Diffraction at Elevated Temperatures, A Method for In situ Process Analysis, John Wiley & Sons, 1993.

[44] J. Molenda, K. Swierczek, W. Zajac, J. Power Sources 173 (2007) 657.

[45] Solid State Ionics 132 (2000) 253.

[46] V.V. Kharton, A.P. Viskup, A.V. Kovalevsky, E.N. Naumovich, F.M.B. Marques, Solid State Ionics 143 (2001) 337.

[47] V.V. Kharton, A.A. Yaremchenko, A.L. Shaula, M.V. Patrakeev, E.N. Naumovich, D.I. Logvinovich, J.R. Frade, F.M.B.J. Marques, Solid State Chem. 177 (2004) 26.